Journal of Materials Chemistry B

ROYAL SOCIETY OF CHEMISTRY

COMMUNICATION

View Article Online
View Journal | View Issue

Cite this: J. Mater. Chem. B, 2025, 13, 1296

Received 2nd August 2024,
Accepted 7th October 2024

DOI: 10.1039/d4tb01712a

rsc.li/materials-b

Dual-responsive micromotor pill for targeted retention in the intestines *in vivo*†

Zitong An, ‡[a] Enguang Lin,‡[b] Zhiguang Wu [c] and Yongming Kang*[d]

There has been considerable interest in the recent advances in synthetic micro/nanomotors in diverse biofluids due to their potential biomedical applications. However, the propulsion of existing micro/nanomotor platforms for delivery in the gastrointestinal (GI) tract is inefficient. Herein, we present a magnetically and chemically actuated micromotor-tableted pill that can be actively retained in the GI tract *in vivo*. A drug-loaded and water-powered magnesium Janus micromotor enveloped in an enteric polymer-protected magnetic pill was stable in the stomach. The movement of the micromotor pill (MP) was promoted using an external gradient alternating magnetic field with low frequency toward the targeted regions in the intestines. An alternating magnetic field with high frequency induces intensive water-powered propulsion of the micromotors though a magnetocaloric effect, and thus effectively prolongs retention in the intestines. The integration of the newly developed MP system enables active retention of micromotors *in vivo* and promises active drug delivery for GI therapy.

1. Introduction

Oral delivery through the gastrointestinal (GI) tract is widely used for the administration of drugs due to its cost effectiveness, high patient compliance, lenient constraints for sterility, and ease of production.[1–3] Recent advances in micro/nanoparticle-based drug delivery systems have demonstrated that their oral administration facilitates survival in the acidic gastric fluids and adequate diffusion into the intestines.[4–6] While effective in accomplishing certain tasks, low efficiency of drug absorption *in vivo* remains a major challenge for practical medical investigations due to the limited intestinal retention time when using the diffusion-based method.[7,8]

Diverse passive diffusion-based targeting strategies have been developed to increase the delivery efficiency at targeted sites, but they remain limited by size constraints and specific surface chemistry. There is an urgent demand for the capability of active navigation of pills in the gastrointestinal (GI) tract to provide active retention of various orally administered therapeutic agents.[9,10] An ideal delivery system in the GI tract is expected to protect the cargos from acidic stomach fluid and transport them to the predetermined site over extended periods to accomplish comprehensive biological tasks.

Over the past decade, there has been great interest in micro- and nanomotors with the capability of navigation into hard-to-reach tissues because they have the potential to empower various biomedical applications, ranging from disease diagnosis to targeted drug delivery.[11–15] Magnesium-based Janus micromotors, in particular, show promising potential in biomedical application *in vivo* due to their efficient water-powered propulsion of gastric and intestinal fluids.[16–19] Their active propulsion increases the retention of cargos in GI tissues. In initial studies *in vivo*, these drug-loaded micromotors were separated in suspension and then orally administered.[20–22] To protect the cargos from acidic pH and enzymatic degradation in the stomach, the micromotors were coated with enteric polymers.[23–26] For a stronger performance in the GI tract, the drug-loaded micromotors were encapsulated into functional pills to extend their life in GI fluids.[27–31] With all these benefits, there is the potential for development of alternating and practical formulations for emerging motor-based drug delivery systems.

Here, we prepared magnetic micromotor pills (MPs) and investigated their magnetically controlled retention using a dynamic gastric delivery platform with prolonged retention (Scheme 1). Ingestible Mg-based micromotors were tableted in enteric protective magnetic pills to prevent etching by gastric acid. The employment of a gradient alternating magnetic field

[a] Imperial College London South Kensington Campus, London, SW7 2AZ, UK
[b] Department of Pathology, Beidahuang Industry Group General Hospital, Harbin, 150081, China
[c] School of Medicine and Health, Harbin Institute of Technology, Harbin, 150006, China
[d] Department of General Surgery, Heilongjiang Provincial Hospital, Harbin, China. E-mail: kangyongming1983@163.com

† Electronic supplementary information (ESI) available. See DOI: https://doi.org/10.1039/d4tb01712a

‡ These authors contributed equally to this work.

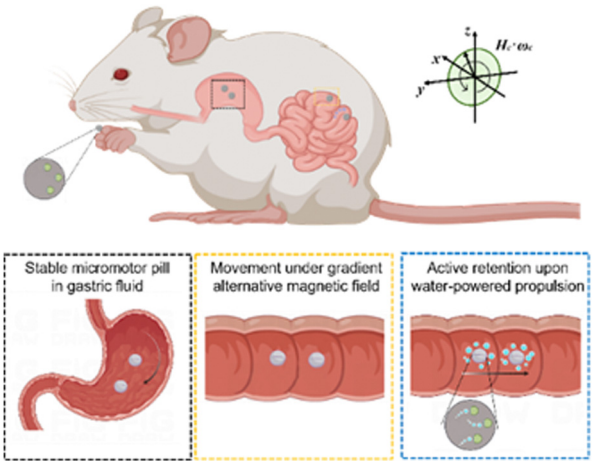

Scheme 1 Conceptional micromotor pill for targeted retention in intestines *in vivo*.

(GAMF) with low frequency (0–50 Hz) promotes the movement of MPs in the GI tract. An alternating magnetic field with high frequency (AMF, 30–100 kHz) induced a magnetocaloric effect of the microcapsules and triggered propulsion of the micromotors, and autonomous and efficient propulsion of the micromotors enhanced the retention in targeted areas of the GI tract. The proposed integrated MP system for oral drug delivery is expected to combine the benefits of therapeutic pill formulations and the active retention of micromotors through magnetic and chemical propulsion, offering an efficient micromotor delivery platform for GI therapies *in vivo*.

2. Experimental

2.1. Materials

Poly(D,L-lactide-*co*-glycolide) (PLGA, $M_w \sim 20\,000$) was purchased from Aladdin Co., Ltd. Magnesium microparticles (20–30 μm) were purchased from Shandong Weigao Co., Ltd. Dulbecco's modified Eagle's medium (DMEM) and phosphate-buffered saline (PBS) buffer solution (pH 7.4) were purchased from Gibco. Gemcitabine (*GEM*) was purchased from Beijing Fanbo Bio-Technology Co., Ltd. Dimethyl sulfoxide (DMSO) was purchased from Beyotime.

2.2. Preparation of GEM-loaded nanoparticles

GEM (3 mL, 8 mg mL^{-1}) was mixed with PLGA (3 mL, 40 mg mL^{-1}) in ethyl acetate, and then sonicated for 15 min. The white solution started to form a W/O/W emulsion when 4 mL of 3% polyvinyl acetate (PVA) was introduced into the mixture upon sonication treatment for 15 min in an ice bath. The W/O/W emulsion was placed into a rotary evaporator (rotation speed of 60 rpm) to evaporate the ethyl acetate at 40 °C. To obtain the GEM-loaded nanoparticles, the emulsion was centrifuged at 5000 for 20 min, and the supernatant was then discarded.

2.3. Preparation of GEM-loaded Mg-based Janus micromotors

First, 5 g of Mg microspheres was washed in ethanol 5 times to remove impurities and MgO. The Mg microspheres were evenly dispersed on glass to form a Mg monolayer. After standing and drying, the surface of the Mg microspheres was coated with 1% PLGA to fix the Mg on the glass. After immobilization, the drug-loaded nanoparticles were modified on the surface of the Mg monolayer. Then, Fe_3O_4 was dissolved in ethanol, and a small watering can was used to deposit layer upon layer of coating on the Mg monolayer. The drug and magnetic nanoparticles were tightly wrapped on the Mg microspheres. Finally, the Mg microspheres were released from the glass, collected in a 1.5-mL centrifuge tube, and sealed. To facilitate the modification of drug-loaded micromotors, GEM was bonded with fluorescein isothiocyanate (FITC). In an ice bath (pH ≈ 9), GEM and FITC at a mass ratio of 1 : 1 were stirred for 24 h, and free FITC was removed by dialysis for 3 days. PLGA was bonded with tetramethylrhodamine isothiocyanate (TRITC) in the same manner and ratio.

2.4. Preparation of micromotor pills

Soluble starch and $NaHCO_3$ were fully ground and then premixed at a mass ratio of 6 : 4 as an auxiliary pill material. The above mixed auxiliary material and magnetic Mg-based Janus micromotors were mixed at a mass ratio of 1 : 1 and placed into a mold for pill pressing. Then, water was added to form pills. After drying, the pressed pills were removed from the mold and immersed in ethanol containing 1% Eudragit L100-55 enteric soluble polymer.

2.5. Detection of cellular reactive oxygen species (ROS)

GEM (0.1 mg mL^{-1}) was co-cultured with 1 mg mL^{-1} Mg-based Janus micromotors and drug-loaded micromotors. After 12 hours of co-culture of different particles with cells, the co-cultured particles were washed off with PBS. In a 96-well plate, 10 μL of DCFH-DA probe was added to each well. After co-culture in a cell incubator for 15 min, the probes that did not enter the cells were washed away with PBS, and the fluorescence of the probes was observed by microscopy. Cellular ROS intensity analysis was performed using ImageJ software.

2.6. Safety evaluation *in vivo*

The mice were dosed *via* the retro-orbital sinuses, and then 24 h later, blood was collected for routine detection. A portion of the blood was incubated at room temperature for 30 min and centrifuged at 4 °C and 5000 rpm for 10 min. The serum was aspirated for liver and kidney function tests.

All the animals were treated in accordance with the Guide for Care and Use of Laboratory Animals. Animal experiments were approved by the Experimental Animal Welfare Ethics Committee of the Harbin Institute of Technology (No. IACUC-2022032).

3. Results and discussion

3.1. Preparation and characterization of MPs

The preparation of MPs mainly consists of two steps: the construction of drug-loaded Mg-based Janus micromotors and the fabrication of MPs (Fig. 1a). To fabricate the Janus Mg-based micromotors, Mg microparticles with an average

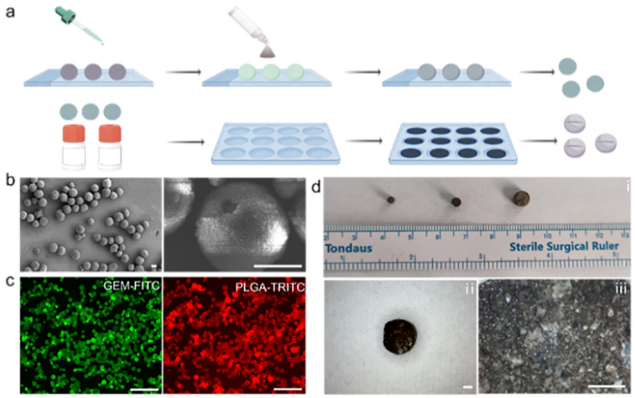

Fig. 1 Preparation and characterization of MPs. (a) Schematic fabrication of Mg-based Janus micromotors and MPs. (b) SEM images of Mg-based Janus micromotors. Scale bars, 20 μm. (c) Fluorescence images of the drug-loaded Mg-based Janus micromotors; GEM was labelled with FITC, and PLGA was labelled with tetramethylrhodamine isothiocyanate (TRITC). Scale bars, 100 μm. (d) Photographs of MPs with different sizes. Scale bars, 500 μm.

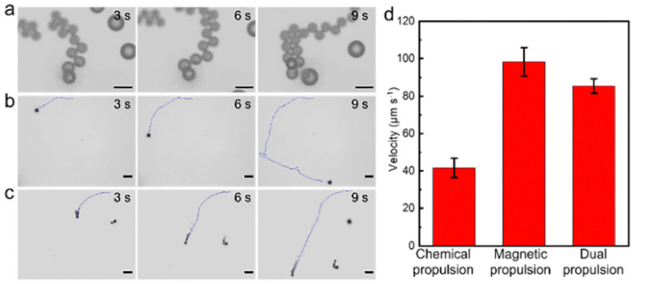

Fig. 2 Chemical and magnetic movement of Mg-based Janus micromotors. (a) Time-lapse images showing the water-powered movement of a Mg-based Janus micromotor in water. (b) Time-lapse images illustrating the motion of a Mg-based Janus micromotor under a magnetic field. (c) Time-lapse images exhibiting the movement of a magnetic Mg-based Janus micromotor through chemical propulsion and magnetic propulsion. (d) Comparison of the velocity of Mg-based Janus micromotors under different propulsion strategies.

diameter of approximately 20 μm were released onto glass slides as the substrate. Subsequently, the poly(lactic-*co*-glycolic acid) (PLGA) layer, which bestows water-powered propulsion in intestinal fluids, was deposited onto the substrate containing the Mg microparticles. An alginate hydrogel layer was coated onto the micromotors by dropping aqueous solution containing alginate, magnetic nanoparticles, and drugs (*e.g.*, GEM) onto the slides. Another PLGA layer was then coated onto the micromotors to serve as a protective scaffold that facilitated stability during their movement.

Fig. 1b shows scanning electron microscopy (SEM) images of GEM-loaded Mg-based micromotors with a spherical geometry and an average diameter of approximately 20 μm. The enlarged SEM images illustrate the small opening (approximately 3 μm in diameter) of the micromotors, which is designed as a catalytic interface for bubble propulsion. The Janus structure of the micromotors with small openings was fabricated through surface contact of the Mg microparticles with substrates during different layer deposition steps. The images in Fig. 1c show that green fluorescence from GEM, which was functionalized with fluorescein isothiocyanate (GEM-FITC), and red fluorescence from PLGA were observed from the micromotors, which verified successful drug loading of the micromotors. Subsequently, the Janus micromotors were tableted into enteric magnetic micromotor capsules (MPs) by the mask-assisted tableting method, and the size of the MPs was controlled through the manipulation of the size of masks. The microscopic images in Fig. 1d show three MPs with diameters of 3 mm, 4 mm, and 6 mm. The resulting micromotor pills included magnetic nanoparticles for magnetic navigation, enteric polymers to prevent etching by stomach fluid, and drug-loaded micromotors.

3.2. Chemical and magnetic movement of Mg-based Janus micromotors

As shown in Fig. 2a and the corresponding Movie S1 (ESI†), the micromotors displayed efficient bubble propulsion in PBS, with a travelling distance of approximately 360 μm in 9 s. The Mg particles without the Janus structure exhibited negligible motion in aqueous media. The efficient water-powered propulsion in the targeted areas in the intestines offers a mechanical effect to increase retention in the intestine. In addition to the chemically powered propulsion, the micromotors also exhibited controllable movement under the AMF with a frequency of 20 Hz. Parameters for the AMF were employed according to peer research on magnetic microrobots upon a GAMF.[32]

The time-lapse images in Fig. 2b, captured from Movie S2 (ESI†), illustrate that the micromotors exhibited orthogonal turning with a minor change in velocity in 9 s. The micromotors were firstly actuated upon by the AMF for 3 s, and then, the external magnetic field was withdrawn (Fig. 2c and Movie S3, ESI†). The micromotors exhibited water-powered propulsion from 3 s to 9 s. Further quantitative analysis indicated that the velocities of the micromotors with chemical and magnetic movement were 41.6 ± 5.3 μm s^{-1} and 98.2 ± 7.7 μm s^{-1}, respectively (Fig. 2d). Such efficient propulsion of the micromotors provides the mechanical driving force for elevated retention and delivery.

3.3. Behaviour of MPs under a magnetic field

Next, the movement behaviour of MPs under a GAMF was characterized. As shown in Fig. 3a, the MPs with a diameter of 3 mm in model intestinal fluid exhibited efficient motion with a nearly linear trajectory upon being subjected to the GAMF. The traveling distance of the MP was approximately 26 mm in 4 s. Similarly, a linear trajectory of MPs with a diameter of 6 mm upon exposure to the GAMF was observed with a distance of approximately 29 mm in 2 s (Fig. 3b). The elevated velocity was attributed to the increased size of the MPs. In contrast, the magnetically actuated motion of the corresponding MPs was decelerated once placed into the murine intestine. The enhanced viscosity in the intestine may cause the deceleration of the MPs (Fig. 3c). The quantitation velocities of the MPs are 6.7 ± 0.8 mm s^{-1} for MPs (3 mm) in intestinal fluid, 18.2 ± 1.1 mm s^{-1} for MPs (6 mm) in intestinal fluid, and 4.0 ± 0.9 mm s^{-1} for MPs (6 mm) in the intestine (Fig. 3d).

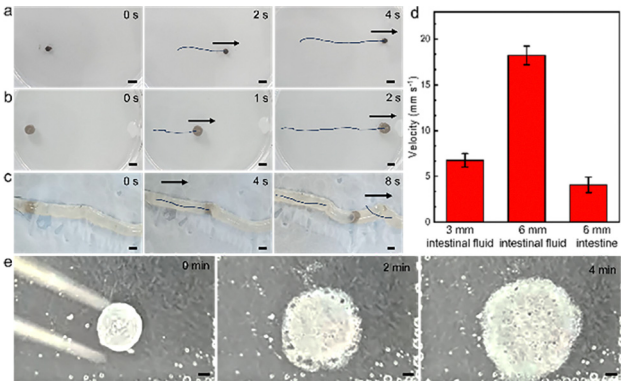

Fig. 3 Behaviour of MPs under a magnetic field. Time-lapse photographic images showing the movement of MPs with diameters of (a) 3 mm and (b) 6 mm in model intestinal fluid under a gradient alternating magnetic field (GAMF). Scale 20 mm. (c) Time-lapse microscopic images displaying the movement of MPs (diameter 6 mm) in model intestinal fluid upon exposure to a GAMF. Scale bar, 2 mm. (d) The velocity of MPs of different sizes in various fluids. (e) Time-lapse photographic images showing the collapse of an MP and the activation of the micromotors upon exposure to an alternating magnetic field with high frequency. Scale bar, 2 mm.

Moreover, the micromotors from MPs were activated through the magnetocaloric effect. Such a magnetocaloric effect also significantly accelerated the Mg–water chemical reactions and thus enhanced the chemical propulsion of the micromotors. As shown in the time-lapse photographs in Fig. 3e, the disintegration of an MP occurred upon application of an alternating magnetic field with a high frequency (frequency: 30 kHz, intensity: 500 mT) for 2 s.

3.4. Active therapy of Mg-based Janus micromotors from MPs *in vitro*

It was reported that the therapeutic mechanism of GEM is mainly attributed to the generation of reactive oxygen species (ROS).[33] Therefore, the therapeutic effect of Mg-based micromotors from MPs was evaluated through the analysis of generated ROS using a DCFH-DA probe, which creates fluorescence upon generation of ROS. Fig. 4a illustrates the fluorescence amplitudes of tumour cells upon treatment of the PBS (control group), free GEM (GEM group), bare Mg-based micromotors (micromotor group), and GEM-loaded Mg-based micromotor (GEM-micromotor group) for 12 hours. The control group appeared to emit low-intensity fluorescence throughout the entire area. In the GEM group, the fluorescence intensity increased compared to that of the control group. Similar to the GEM group, the fluorescence signal in the micromotor group showed a higher intensity compared with the control group. Notably, the fluorescence signal in the GEM-micromotor group was higher than those of the other groups.

To quantitatively estimate the amount of ROS received by the tumour cells, the amplitude values from the above fluorescence images were used. As shown in Fig. 4b, the GEM-micromotor group exhibited the highest fluorescence amplitude of 27.6. The fluorescence amplitudes from the micromotor group and the GEM group displayed the values of 10.0 and 8.0,

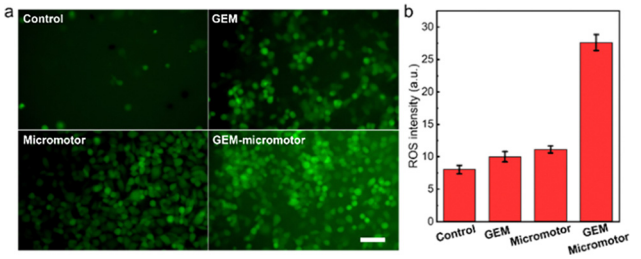

Fig. 4 Active therapy of Mg-based Janus micromotors from MPs against cancer cells *in vitro*. (a) Fluorescence microscopic images showing the intracellular ROS in PANC-1 pancreatic ductal adenocarcinoma cells upon different treatments. (b) Corresponding DCF^{+} cell ratio upon different treatments.

respectively. The near 3-fold elevation in DCF-positive tumour cells clearly demonstrates that the Mg-based micromotors can effectively alter the oxidative stress state of tumour cells. This is largely due to the combined effect of the release of GEM and the generation of H_2 from the Mg-based Janus micromotors. Therefore, the above data involving the detection of ROS indicates the therapeutic effects of the Mg-based micromotors.

3.5. Distribution of MPs *in vivo*

To evaluate the capability of the MPs for targeted retention at predefined segments of the intestine *in vivo*, four groups of mice were assigned to compare dual-responsive MPs with free GEM, GEM-loaded micromotors, and MPs without an alternating magnetic field. To this end, the mice were euthanized, and their stomach and entire GI tract were removed to evaluate the biodistribution and retention of the MPs upon exposure to a magnetic field. As shown in Fig. 5a, the image obtained from the GI tract collected at 4 h showed the strongest fluorescence in the jejunum. In contrast, PBS containing GEM and GEM-loaded micromotors was orally administered to the mice. A minor fluorescence signal was detected in the intestine, and the predominant fluorescence signal was located in the stomach, which may be attributed to the self-fluorescence from food. The treatment of MPs without a magnetic field resulted in a significantly lower fluorescence intensity compared to the treatment of MPs + AMF, reflecting their greatly reduced retention in the jejunum under the same experimental conditions and coatings.

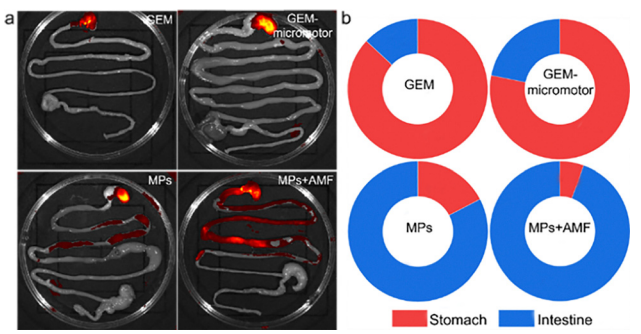

Fig. 5 Distribution of MPs *in vivo*. (a) Distribution in the gastrointestinal tract of mice 4 hours after oral administration. (b) Proportion of distribution in the gastrointestinal tract of mice 4 hours after oral administration.

The corresponding quantification analysis displays the location of 13.1% and 21.8% in the intestine for the GM and Pill groups, respectively (Fig. 5b). The treatment administered to the MP group resulted in the distribution of 54.2% in the intestine. In contrast, 94.5% of the MPs + AMF group were controlled in the intestine upon manipulation of the magnetic field. Overall, the MPs with self-propelled micromotors led to improved localized retention of their payloads in the intestine compared to passive diffusion. It should be noted that the enhanced distribution of MPs under AMF may not exclusively be attributed to the magnetically actuated movement. It has been reported that the magnetic actuation of magnetic cargos in the intestine may also stimulate intestinal peristalsis,[34] which may play an important role in the movement of MPs upon exposure to an AMF.

3.6. Safety evaluation of MPs *in vivo*

Finally, the safety profile of the MPs in the GI tract was estimated. PBS buffer and a suspension of MPs were orally administered to the mice, and they were monitored for general toxicity signs 4 hours post-administration. Histological analysis using a hematoxylin and eosin (H&E) pathological staining assay was performed to further evaluate the toxicity of the MPs *in vivo* (Fig. 6a). The major organs were harvested from mice in the above-mentioned eight models for H&E staining analysis. In contrast to the PBS group, no pathological abnormalities or inflamed cells in the brain, heart, liver, spleen, lung, or kidney were observed in the treated model groups, demonstrating the negligible toxicity of MPs in the mice. Moreover, a comprehensive analysis of the blood chemistry panel and major blood cell populations was conducted for the samples 4 h after oral administration (Fig. 6b).

The biomarkers indicating liver function *in vivo*, including the activity of alanine aminotransferase (ALT) and aspartate aminotransferase (AST) and the content of globulin (GLOB), were studied through the collection of blood samples of mice injected with MPs. Urea and serum creatinine (CREA) are markers of renal function. Compared with the control group, the levels of all serum biochemistry markers and numbers of red blood cells in the mice upon treatment with MPs remained at normal levels. These results indicate that the MPs are safe to utilize for oral administration of various therapeutic agents. Other types of micromotors, such as mesoporous silica-based micromotors, can also be used to activate delivery of various therapeutic agents with minor toxicity according to a recent report.[35]

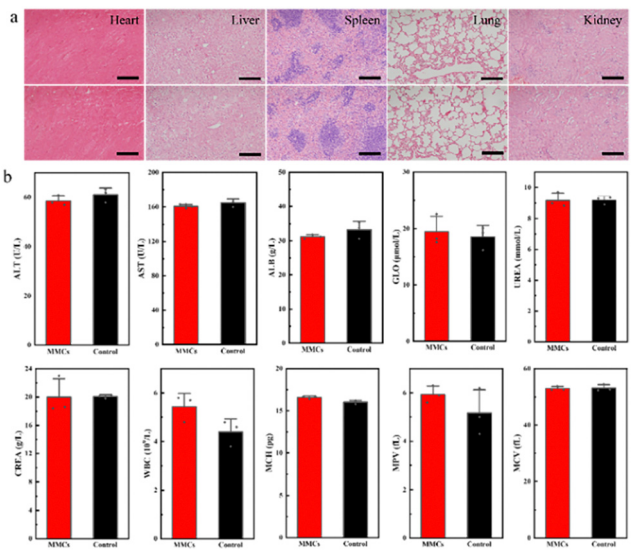

Fig. 6 Safety evaluations of MPs *in vivo*. (a) HE-stained sections of the heart, liver, spleen, lung, and kidney of mice after administration. (b) Liver function, renal function, and blood routine indexes of mice after administration.

4. Conclusions

We developed an ingestible micromotor tablet designed for energetic retention manipulation within the intestines. These drug-encapsulated micromotors were tableted into drugs with controllable sizes. The micromotor pills (MPs) allow controlled motion *via* each magnetic propulsion and chemical propulsion mechanism in various biofluids. To accomplish a predetermined task, the MPs are activated through the utility of an outside alternating magnetic force. The magnetocaloric impact initiates the propulsion of the water-powered micromotors, thereby controlling their retention within the gastrointestinal tract. Although the concept of the MPs is in its early stages with regard to the magnetic control inside the GI tract, similar studies will increase our understanding of the magnetic navigation of such micromotor platforms under real-time imaging systems. We envision that those robust structures will facilitate the suitable localized delivery of numerous therapies, and will advance *in vivo* biomedical programs.

Author contributions

ZTA: completed experiments, collected and organized the data. EGL: completed experiments, collected and organized the data. ZGW: wrote the article. YMK: designed and funded the experiments.

Data availability

The data that support the findings of this study are available from the corresponding author upon reasonable request.

Conflicts of interest

There are no conflicts to declare.

References

1 M. S. Alqahtani, M. Kazi, M. A. Alsenaidy and M. Z. Ahmad, *Front. Pharmacol.*, 2021, **12**, 618411.
2 S. Hua, *Front. Pharmacol.*, 2020, **11**, 524.
3 J. N. Chu and G. Traverso, *Nat. Rev. Gastroenterol. Hepatol.*, 2022, **19**, 219–238.

4 A. M. Bellinger, M. Jafari, T. M. Grant, S. Zhang, H. C. Slater, E. A. Wenger, S. Mo, Y.-A. L. Lee, H. Mazdiyasni and L. Kogan, *Sci. Transl. Med.*, 2016, **8**, 365ra157.
5 R. Ahmad, S. Srivastava, S. Ghosh and S. K. Khare, *Colloids Surf. B*, 2021, **197**, 111389.
6 F. Sabbagh and B. S. Kim, *J. Controlled Release*, 2022, **341**, 132–146.
7 W. Shan, X. Zhu, M. Liu, L. Li, J. Zhong, W. Sun, Z. Zhang and Y. Huang, *ACS Nano*, 2015, **9**, 2345–2356.
8 J. Zhou, M. Li, Q. Chen, X. Li, L. Chen, Z. Dong, W. Zhu, Y. Yang, Z. Liu and Q. Chen, *Nat. Commun.*, 2022, **13**, 3432.
9 A. Mercado-Perez and A. Beyder, *Nat. Rev. Gastroenterol. Hepatol.*, 2022, **19**, 283–296.
10 M. Koziolek, M. Grimm, F. Schneider, P. Jedamzik, M. Sager, J.-P. Kühn, W. Siegmund and W. Weitschies, *Adv. Drug Delivery Rev.*, 2016, **101**, 75–88.
11 A. Aziz, M. Medina-Sánchez, N. Koukourakis, J. Wang, R. Kuschmierz, H. Radner, J. W. Czarske and O. G. Schmidt, *Nano Lett*, 2019, **29**, 1905272.
12 B. Esteban-Fernández de Ávila, P. Angsantikul, J. Li, W. Gao, L. Zhang and J. Wang, *Adv. Func. Mater.*, 2018, **28**, 1705640.
13 M. Sitti, *Nat. Rev. Mater.*, 2018, **3**, 74–75.
14 Y. Alapan, O. Yasa, O. Schauer, J. Giltinan, A. F. Tabak, V. Sourjik and M. Sitti, *Sci. Rob.*, 2018, **3**, eaar4423.
15 F. Novotný, H. Wang and M. Pumera, *Chem*, 2020, **6**, 867–884.
16 F. Mou, C. Chen, H. Ma, Y. Yin, Q. Wu and J. Guan, *Angew. Chem., Int. Ed.*, 2013, **52**, 7208–7212.
17 C. Chen, E. Karshalev, J. Guan and J. Wang, *Small*, 2018, **14**, 1704252.
18 F. Zhang, R. Mundaca-Uribe, H. Gong, B. Esteban-Fernández de Ávila, M. Beltrán-Gastélum, E. Karshalev, A. Nourhani, Y. Tong, B. Nguyen, M. Gallot, Y. Zhang, L. Zhang and J. Wang, *Adv. Mater.*, 2019, **31**, 1901828.
19 C. Xu, S. Wang, H. Wang, K. Liu, S. Zhang, B. Chen, H. Liu, F. Tong, F. Peng, Y. Tu and Y. Li, *Nano Lett.*, 2021, **21**, 1982–1991.
20 W. Gao, R. Dong, S. Thamphiwatana, J. Li, W. Gao, L. Zhang and J. J. Wang, *ACS Nano*, 2015, **9**, 117–123.
21 J. Li, S. Thamphiwatana, W. Liu, B. Esteban-Fernández de Avila, P. Angsantikul, E. Sandraz, J. Wang, T. Xu, F. Soto and V. J. A. N. Ramez, *Angew. Chem., Int. Ed.*, 2016, **10**, 9536–9542.
22 B. E.-F. de Ávila, P. Angsantikul, J. Li, M. A. Lopez-Ramirez, D. E. Ramírez-Herrera, S. Thamphiwatana, C. Chen, J. Delezuk, R. Samakapiruk and V. J. N. C. Ramez, *Nat. Commun.*, 2017, **8**, 272.
23 J. Li, P. Angsantikul, W. Liu, B. Esteban-Fernández de Ávila, S. Thamphiwatana, M. Xu, E. Sandraz, X. Wang, J. Delezuk and W. Gao, *Angew. Chem., Int. Ed.*, 2017, **56**, 2156–2161.
24 Z. Wu, L. Li, Y. Yang, P. Hu, Y. Li, S.-Y. Yang, L. V. Wang and W. Gao, *Sci. Rob.*, 2019, **4**, eaax0613.
25 F. Zhang, Z. Li, Y. Duan, A. Abbas, R. Mundaca-Uribe, L. Yin, H. Luan, W. Gao, R. H. Fang and L. Zhang, *Sci. Rob.*, 2022, **7**, eabo4160.
26 H. Choi, S. H. Jeong, T. Y. Kim, J. Yi and S. K. Hahn, *Bioact. Mater.*, 2022, **9**, 54–62.
27 E. Karshalev, B. Esteban-Fernández de Ávila, M. Beltrán-Gastélum, P. Angsantikul, S. Tang, R. Mundaca-Uribe, F. Zhang, J. Zhao, L. Zhang and J. Wang, *ACS Nano*, 2018, **12**, 8397–8405.
28 R. Mundaca-Uribe, N. Askarinam, R. H. Fang, L. Zhang and J. Wang, *Nat. Biomed. Eng*, 2023, 1–13.
29 L. Děkanovský, J. Li, H. Zhou, Z. Sofer and B. Khezri, *Energies*, 2022, **15**, 426.
30 Y. Wang, J. Shen, S. Handschuh-Wang, M. Qiu, S. Du and B. Wang, *ACS Nano*, 2023, **17**, 27–50.
31 A. K. Dhalla, Z. Al-Shamsie, S. Beraki, A. Dasari, L. C. Fung, L. Fusaro, A. Garapaty, B. Gutierrez, D. Gratta and M. Hashim, *Drug Deliv. Transl. Re*, 2022, 1–12.
32 H. Xie, M. Sun, X. Fan, Z. Lin, W. Chen, L. Wang, L. Dong and Q. J. S. R. He, *Sci. Rob.*, 2019, **4**, eaav8006.
33 C. Wang, J. Wang, X. Zhang, S. Yu, D. Wen, Q. Hu, Y. Ye, H. Bomba, X. Hu and Z. Liu, *Sci. Transl. Med.*, 2018, **10**, eaan3682.
34 K. B. Ramadi, J. C. McRae, G. Selsing, A. Su, R. Fernandes, M. Hickling, B. Rios, S. Babaee, S. Min and D. Gwynne, *Sci. Rob.*, 2023, **8**, eade9676.
35 E. Guzmán and A. Maestro, *Technologies*, 2022, **10**, 96.